Received 14 March 2024; accepted 1 April 2024. Date of publication 16 April 2024; date of current version 3 May 2024.

Digital Object Identifier 10.1109/OJCOMS.2024.3389093

Sum Rate and Fairness Optimization in RIS-Assisted VLC Systems

SALAH ABDELJABAR (Student Member, IEEE), MAHMOUD WAFIK ELTOKHEY (Member, IEEE), AND MOHAMED-SLIM ALOUINI (Fellow, IEEE)

Division of Computer, Electrical and Mathematical Science and Engineering (CEMSE), King Abdullah University of Science and Technology (KAUST), Thuwal 23955, Saudi Arabia

CORRESPONDING AUTHOR: M. W. ELTOKHEY (e-mail: MAHMOUD.ELTOKHEY@KAUST.EDU.SA)

ABSTRACT The use of visible light communication (VLC) to support wireless coverage has been receiving increasing interest, due to factors that include its operation in a large unregulated spectrum and immunity against electromagnetic interference. On the other hand, the sensitivity of VLC network performance to the line-of-sight (LOS) link quality affects the system reliability. The emergence of reconfigurable intelligent surfaces (RISs) in optical domain opens the door for minimizing the impacts of the LOS link degradation on VLC networks, given the possibilities they provide for enhancing the non-LOS channel gain. In this paper, we propose optimizing the RIS-assisted VLC systems by controlling the RIS elements to maximize the network sum-rate while maintaining fairness in the user achievable throughput. Two types of RIS elements are considered, where the addressed non-convex optimization problems are handled using the genetic algorithm and the particle swarm optimization techniques, presenting improvement in network performance in terms of sum rate, fairness, and link outage ratio. In addition, we investigate the RIS-assisted VLC system performance in cases of handling mobile users, highlighting the trade-off between the variation in the optimization rate and the network performance.

INDEX TERMS Visible light communication, reconfigurable intelligent surfaces, multi-objective optimization, genetic algorithm, particle swarm optimization.

I. INTRODUCTION

With the ever-increasing demand for broadband connectivity, reliance on optical wireless communication technologies for complementing the already-congested radio frequency (RF) spectrum has been receiving a growing interest. In indoor areas where light-emitting diode (LED)-based luminaires are widely deployed, supporting simultaneous lighting and data transfer using visible light communication (VLC) offers interesting solutions for providing wireless coverage, benefiting from large unregulated spectrum, capabilities to achieve high link rates, immunity to electromagnetic field (EMF) interference, and efficiency in resource utilization [1]. On the other hand, due to the significant contributions of the line-of-sight (LOS) components to the VLC channel gain, the VLC links are sensitive to the LOS link blockage and shadowing as well as the misalignments between the transmitters (Txs) and the receivers (Rxs) [1].

The interest in the utilization of reconfigurable intelligent surfaces (RISs) in VLC networks has been growing recently, given their capabilities to induce controlled changes in the VLC channel by varying the parameters of the incident signals [2]. In particular, the use of RIS arrays in VLC networks enables increasing the achievable network throughput and minimizing the impacts of LOS link blockage and shadowing by enhancing the non-LOS (NLOS) channel gain. This could help in improving the VLC link quality and reliability [3], according to the characteristics of the used RIS array [4], [5], [6]. Based on the response induced by the RIS elements to the impinging light signals, optical RISs can be classified into specular reflecting, diffuse reflecting, and refracting RISs [4]. Among these types, specular reflecting RISs and diffuse reflecting RIS are of special interest for indoor VLC systems. Specular reflecting RISs can be realized by use of elements that specularly reflect the incident signals (e.g., mirror arrays), while diffuse reflecting RISs are

realizable using Lambertian reflecting surfaces. Note that, it was shown in [7] that the utilisation of RISs with a size of 25 cm $\times$ 15 cm in a VLC system can increase the received power by a factor of up to five when compared to relying only on the LOS links, which highlights their effectiveness in enhancing the system performance in presence of LOS links [7], [8]. In general, harnessing the full potential of the RISs necessitates efficient optimization of the RIS elements to adapt to the changes in the communications environment, where the choice of the RIS elements impacts how the RIS array affects the network performance [4]. In that regard, several works in literature investigated the optimization of RISs in indoor VLC systems for improving the achievable throughput [9], [10], [11], [12], [13], [14], [15], [16], [17], bit-error-rate (BER) [18], [19], mean-squared-error (MSE) [20], and secrecy performance [21], [22], [23], [24]. In [9], Sine-Cosine algorithm was utilized for optimizing the RIS elements to maximize the achievable network throughput, while [10] studied the RIS array optimization in non-orthogonal multiple access (NOMA)-based systems. Also, in [11], the maximization of the achievable network throughput under the point source assumption for the NLOS channel model was investigated using greedy policy algorithm, while [12] studied the maximization of the spectral efficiency of time-division-multiple-access (TDMA) system under the same assumption using alternating optimization and frozen-variable algorithm. The works in [13] and [14] investigated maximizing the achievable throughput using particle swarm optimization (PSO), where [13] optimized the position of the RIS elements and [14] optimized the assignment of the elements in multiple-input multiple-output (MIMO) setup. In addition, [15] proposed a hybrid NOMA scheme for improving the RIS-assisted VLC system capacity, while [16] studied improving the asymptotic capacity of the multiple-input single-output (MISO) RIS-aided VLC systems by utilizing the theory of quadratic programming. The work in [17] proposed a two-stage deep Q-learning-based resource management framework for RIS-assisted VLC systems to maximize the possible fairness among users and the overall spectral efficiency. The authors in [18] studied the use of RISs to improve link reliability in VLC systems using NOMA, proposing a joint optimization framework based on the genetic algorithm (GA), while the authors in [19] studied maximizing the average BER for RIS-based VLC system, and the authors in [20] explored minimizing the MSE of MIMO VLC systems. For improving secrecy performance, [21] studied the use of RISs to improve secrecy capacity of NOMA VLC systems, solving the formulated problem using GA, while [22] investigated the problem of maximizing the secrecy capacity using PSO for RIS-assisted VLC systems considering one legitimate user and one eavesdropper. Also, a deep reinforcement learning (DRL) framework was proposed in [23] for an RIS-assisted VLC to maximize secrecy capacity, while in [24] the authors explored maximizing the secrecy capacity, proposing an iterative Kuhn-Munkres technique to solve the formulated problem.

Due to the large contributions of the LOS components to the VLC channel gain, which are inversely proportional to the square of link distances, the users performances in VLC networks are highly impacted by their locations and orientations. Indeed, this may reflect in large performance gaps between users, represented by degradations in terms of fairness between the individual user achievable throughput performances, and could affect the link reliability. Although the works in [9], [10], [11], [12], [13], [14], [15], [16], [18], [19], [20], [21], [22], [23], [24] focused on improving the network performance, the fairness between individual user performances was not considered. Note that, the work in [17] considered optimization of fairness along with spectral efficiency, however, optimization was carried out sequentially, only specular reflecting RISs were optimized, and user mobility was not considered. In this paper, we propose optimizing the RISs in indoor VLC systems to improve the system performance by simultaneous maximization of the network sum rate and fairness while accounting for user mobility, which to the best of our knowledge was not considered before. In addition, to address different network needs by benefiting from the characteristics of the used RIS arrays, two types of RIS elements are considered, where we formulate for each RIS type a multi-objective optimization problem. Due to the non-convexity of the handled optimization problems, we utilize the GA and the PSO techniques, which have been considered for solving range of problems in the area of optical wireless communications [18], [22], [25], [26], [27]. Table 1 compares the paper to the related works in literature. The main contributions can be summarized as follows:

- proposing multi-objective optimization of RISs in indoor VLC networks to simultaneously maximize the network sum rate and the fairness between individual user performances while considering random Rx orientations;
- studying the optimization of different types of RISs, highlighting the impact of the characteristics of the used RIS elements on sum rate and fairness;
- proposing optimization of RIS elements while accounting for user mobility, highlighting the trade-off between the optimization rate (complexity) and system performance.

The rest of the paper is organized as follow: In Section II the system parameters are described, where the considered types of RISs are discussed. Then, the multi-objective utility function and the proposed optimization schemes for different RIS types are explained in Section III. Afterwards, simulation results are presented for evaluating the performance of the proposed schemes in Section IV, before concluding the paper in Section V.

TABLE 1. List of works that consider optimization of reflecting RIS elements in indoor VLC networks in terms of mean square error (MSE), bit-error rate (BER), fairness index (FI), and rate.

[#]	RIS Type		Objective functions					Rx Configuration	
	Specular	Diffuse	MSE	BER	Secrecy Rate	Rate	FI	Random Device Orientation	User Mobility
[9]		✓				✓		✓	
[10]	✓					✓			
[11]	✓					✓			
[12]	✓					✓			
[13]	✓					✓			
[14]	✓					✓			
[15]	✓					✓			
[16]		✓				✓			
[17]	✓					✓	✓	✓	
[18]	✓			✓				✓	
[19]		✓		✓					
[20]	✓		✓						
[21]	✓				✓				
[22]	✓				✓				
[23]	✓				✓				✓
[24]	✓				✓				
This paper	✓	✓				✓	✓	✓	✓

NOTATIONS

Throughout the paper, vectors are represented by use of lower-case bold letters ($\mathbf{a}$), while matrices are denoted by use of upper-case bold letters ($\mathbf{A}$). Furthermore, $\odot$ and $\mathbb{R}_+$ represent the Hadamard product and the set of real and positive numbers, respectively.

II. SYSTEM MODEL

We consider a MISO indoor environment with N_t LED-based fixtures acting as Txs and N_r Rxs, each equipped with a single photodetector (PD), where a square RIS array comprising N_{RIS} elements is placed on one of the room walls to assist the downlink transmission as shown in Fig. 1. We assume broadcasting the same signals by all Txs with equal distribution of the time resources in a TDMA system. The Txs and the RIS elements are linked to a central control unit, which is responsible for information exchange and carrying out the main computational operations. The channel state information (CSI) estimation can be carried out with the aid of pilot symbols transmission from the Txs, where infrared-based uplinks could be considered for data transmission from the user devices [28].

A. CHANNEL GAIN OF LOS PATHS

Assuming intensity modulation direct detection system with Lambertian transmission by the LED luminaires, the VLC channel gain (excluding the impacts of blocking, shadowing, and the reflections from the RISs) between the l^{th} Tx and the r^{th} Rx, $h_{l,r}$, is dominated by the LOS component, which is given by [1], [29]:

$$h_{l,r}^{\text{LOS}} = \frac{1}{2\pi}\frac{(m+1)A_r\xi_r}{d_{l,r}^2}\cos^m\left(\Phi_{l,r}\right)\cos\left(\theta_{l,r}\right)g\left(\theta_{l,r}\right), \quad (1)$$

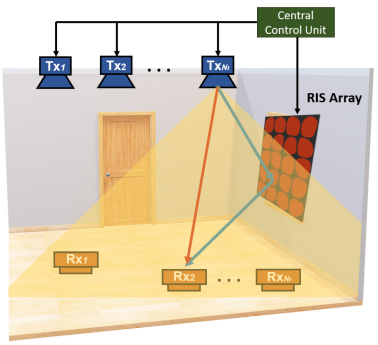

FIGURE 1. Illustration for the considered VLC system where RIS array assists the downlink transmission from the LED-based fixtures to the Rxs.

where m is the Lambertian order, and A_r and ξ_r denote the r^{th} Rx PD area and responsivity, respectively. Also, $d_{l,r}$ is the distance of the link, while $\Phi_{l,r}$ and $\theta_{l,r}$ denote the emission angle with respect to the l^{th} Tx and the incidence angle with respect to the r^{th} Rx, respectively, as illustrated in Fig. 2. The optical concentrator gain at the r^{th} Rx is represented by $g(\theta_{l,r})$ such that [30]:

$$g\left(\theta_{l,r}\right) = \begin{cases} \frac{n_{\text{i}}^2}{\sin^2(\Psi_{\text{FOV}})}, & 0 \le \theta_{l,r} \le \Psi_{\text{FOV}} \\ 0, & \theta_{l,r} > \Psi_{\text{FOV}} \end{cases}, \quad (2)$$

where n_{i} and Ψ_{FOV} denote the refractive index of the optical concentrator and the semi-angle of the Rx field-of-view (FOV), respectively. To simplify the notation, we define a vector that combines the channel gains between the r^{th} Rx and all Txs, which is denoted by:

$$\mathbf{h}_{\text{LOS},r} = \left[h_{1,r}^{\text{LOS}}, \ldots, h_{N_t,r}^{\text{LOS}}\right]^T; \mathbf{h}_{\text{LOS},r} \in \mathbb{R}_+^{N_t \times 1}. \quad (3)$$

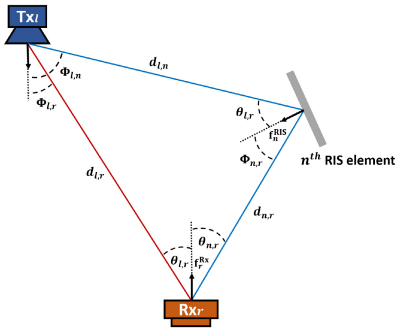

FIGURE 2. The main geometric parameters of the RIS-assisted VLC system.

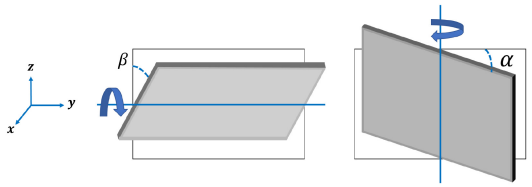

FIGURE 3. Illustration of RIS elements controlled by variation of the yaw (α) and roll (β) rotational angles.

B. CHANNEL GAIN OF THE REFLECTED PATH VIA RIS

The RISs are structures that can be adapted to induce variations in the incident waves propagation for controlling the network performance [2]. The utilization of RISs in VLC networks enables strengthening the link quality and robustness by introducing enhancements in the NLOS channel gain, which depends on the characteristics of the elements used for building the RIS array [4]. In general, the RIS elements in the optical domain can be classified according to their impact on directing the incident signals into reflecting and refracting elements [4], [5], [6]. In this work we consider the use of reflecting elements, which can rely on specular or diffuse reflections for directing the incident signals, and evaluate the advantages provided by each type. Such RIS elements could be controlled by varying their orientations within the yaw and roll rotational angles, as shown in Fig. 3. By considering a local reference Cartesian coordinate at the RIS array plane, the normal vector to the n^{th} RIS element, $\mathbf{f}_n^{\text{RIS}}$, can be expressed with respect to its azimuth (roll) and polar (yaw) angles as:

$$\mathbf{f}_n^{\text{RIS}} = [\sin(\beta)\cos(\alpha), \quad \sin(\beta)\sin(\alpha), \quad \cos(\beta)]^T. \quad (4)$$

1) SPECULAR REFLECTING RIS

This type of RISs can be realized by use of surfaces that specularly reflect the incident signals following Snell's law (e.g., mirrors controlled by rotary motors), where the reflection angles could be varied by manipulating the orientations of the RIS elements [31]. Note that, the intensity of the reflected signals are attenuated by a factor that depends on the characteristics of the RIS element. Also, due to the size of the RIS elements and the separations between the Txs and Rxs in VLC scenarios, it is assumed that the reflected beam footprint in the Rx plane has a limited coverage that allows each specular reflecting RIS element to serve only one Tx and one Rx at a time [11], [12]. Given the large sizes of the assumed RIS elements compared to the signal wavelength and that the distances between the VLC Txs and RIS elements are relatively large, the radiometry-based approach in [7] is considered for assessing the contributions of the reflected signals to the channel gain, where the channel gain, under the point source assumption, at the r^{th} Rx of the transmission by the l^{th} Tx reflected via the n^{th} RIS element is given by [7], [32]:

$$h_{l,n,r}^{\text{NLOS}} = \frac{1}{2\pi}\delta_n \frac{(m+1)A_r\xi_r}{(d_{l,n}+d_{n,r})^2}\cos^m(\Phi_{l,n})\cos(\theta_{n,r})g(\theta_r), \quad (5)$$

where δ_n is the reflection coefficient of the n^{th} RIS element, $d_{l,n}$ is the distance of the link from the Tx to the RIS element, and $d_{n,r}$ is the distance of the link from the RIS element to the Rx. Also, $\Phi_{l,n}$ represents the emission angle of the link from the Tx to the RIS element, while $\theta_{n,r}$ denotes the incidence angle of the link from the RIS element to the Rx. Since each specular reflecting RIS element is assumed to serve only one Tx and one Rx at a time, we introduce two discrete matrices $\mathbf{Q}$ and $\mathbf{Z}$ to represent the associations of the RIS elements with the Txs and Rxs, respectively [20]. Here, the matrices $\mathbf{Q} \triangleq [\mathbf{q}_1, \ldots, \mathbf{q}_{N_t}] \in \{0,1\}^{N_{\text{RIS}}\times N_t}$ and $\mathbf{Z} \triangleq [\mathbf{z}_1, \ldots, \mathbf{z}_{N_r}] \in \{0,1\}^{N_{\text{RIS}}\times N_r}$. Particularly, $q_{n,l} = 1$ and $z_{n,r} = 1$ refer to the association of the n^{th} RIS element with the l^{th} Tx and the r^{th} Rx. The vector of the channel gains of the components reflected via the RIS array towards the r^{th} Rx are then given by:

$$\mathbf{h}_{\text{RIS},r}^{\text{Specular}} = \left[(\mathbf{q}_1 \odot \mathbf{z}_r)^T\mathbf{h}_{1,r}^{\text{RIS}}, \ldots, (\mathbf{q}_{N_t} \odot \mathbf{z}_r)^T\mathbf{h}_{N_t,r}^{\text{RIS}}\right]^T;$$
$$\mathbf{h}_{\text{RIS},r}^{\text{Specular}} \in \mathbb{R}_+^{N_t\times 1}, \quad (6)$$

where $\mathbf{h}_{l,r}^{\text{RIS}} \triangleq [h_{l,1,r}^{\text{NLOS}}, \ldots, h_{l,N_{\text{RIS}},r}^{\text{NLOS}}] \in \mathbb{R}_+^{N_{\text{RIS}}\times 1}$. As a result of the mentioned assumptions, finding the association behaviour (which VLC Tx and Rx each RIS element would serve) could be realized to characterize its operation. Once the association is known, a reverse look-up table is used to obtain the required yaw and roll angles to allow the ray generated via Tx l to serve Rx r.

2) DIFFUSE REFLECTING RIS

Such type of RISs can be realized by using surfaces that diffusely reflect the incident signals [8], where the characteristics of the reflected signals depend on factors such as the orientation and reflectivity of the reflecting element [4]. Assuming reflection by the RIS elements following the Lambertian reflection model, the reflected components will be scattered, where the channel gain of the diffuse reflected component for l^{th} Tx transmission arriving at the r^{th} Rx through the n^{th} RIS element is given by [9], [29]:

$$h_{l,n,r}^{\text{NLOS}} = \frac{1}{2\pi}\rho_n \frac{(m+1)A_rA_n\xi_r}{(d_{l,n})^2(d_{n,r})^2}\cos^m(\Phi_{l,n})\cos(\theta_{l,n})$$
$$\times \cos(\Phi_{n,r})\cos(\theta_{n,r})g(\theta_r), \quad (7)$$

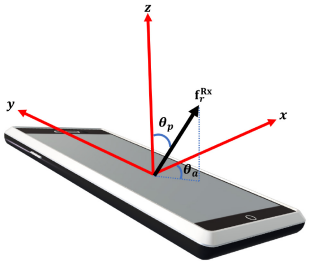

FIGURE 4. Illustration for device orientation with respect to the azimuthal angle θ_a and the polar angle θ_p [33].

where ρ_n and A_n represent the reflectivity and the area of the n^{th} RIS element, respectively. In addition, $\theta_{l,n}$ denotes the angle of incidence of the link from the Tx to the RIS element, while $\Phi_{n,r}$ is the angle of emission of the link from the RIS element to the Rx. Since the components reflected by the RIS elements are diffused, they have wider coverage at the Rx plane, which reduces the dependency on accurate localization of the Rx to ensure receiving the NLOS components. However, this comes at the expense of reduced channel gain compared to the specular reflecting RISs (see the contribution of the distance term in the denominator of (5) and (7)). Given the transmission characteristics of the diffuse reflecting RIS elements and the absence of need for associating the RIS elements to specific Txs and Rxs, the vector of the channel gains of the reflected components by the RIS array at the r^{th} Rx can be expressed as:

$$\begin{aligned}&\mathbf{h}_{\text{RIS},r}^{\text{Diffuse}} = \left[\mathbb{1}^T\mathbf{h}_{1,r}^{\text{RIS}}, \ldots, \mathbb{1}^T\mathbf{h}_{N_t,r}^{\text{RIS}}\right]^T;\\ &\mathbf{h}_{\text{RIS},r}^{\text{Diffuse}} \in \mathbb{R}_{+}^{N_t\times 1},\end{aligned} \tag{8}$$

where $\mathbb{1}$ represents a vector of all entries equal to one.

C. RANDOM DEVICE ORIENTATION

To account for the impact of handling Rxs with random orientations, we consider the model in [33], where the Rx normal vector is characterized by the azimuthal angle θ_a and the polar angle θ_p. Here, θ_a follows a uniform distribution, $\theta_a \sim \mathbb{U}[-\pi, \pi]$, while θ_p follows truncated Laplace distribution with the following probability density function [33]:

$$f_{\theta_p} = \frac{\exp\left(-\frac{\left|\theta_p - \varrho_{\theta_p}\right|}{b_{\theta_p}}\right)}{2b_{\theta_p}}, \quad 0 \le \theta_p \le \frac{\pi}{2}, \tag{9}$$

where ϱ_{θ_p} and b_{θ_p} are the mean and variance of θ_p, respectively. As shown in Fig. 4, the normal vector at the plane of the Rx can be expressed with respect to the polar and azimuthal angles as follows:

$$\mathbf{f}_r^{\text{Rx}} = \left[\sin(\theta_p)\cos(\theta_a), \quad \sin(\theta_p)\sin(\theta_a), \quad \cos(\theta_p)\right]^T. \tag{10}$$

III. SUM RATE AND FAIRNESS MAXIMIZATION PROBLEM

To improve the system performance in terms of user achievable throughput and fairness we consider maximizing the sum rate and fairness index (FI), which provides an indication of the homogeneity between the user performances across the RIS-assisted VLC network. For calculating the user achievable throughput, we adopt the expression derived in [34], given the unique characteristics of the VLC systems due to factors that include dealing with non-negative and real signals. The achievable throughput for the r^{th} Rx in the RIS-assisted VLC system can be expressed as [12], [34]:

$$R_r = \frac{B}{2N_r}\log_2\left(1 + \frac{e}{2\pi}\text{SNR}_r\right), \tag{11}$$

where e is the natural exponential constant, and SNR_r refers to the signal-to-noise-ratio at the r^{th} Rx, which is given by:

$$\text{SNR}_r = \frac{(P_T\hbar_r)^2}{\mathcal{N}B}, \tag{12}$$

$$\hbar_r = \mathbb{1}^T\mathbf{h}_{\text{LOS},r} + \mathbb{1}^T\mathbf{h}_{\text{RIS},r}^{\{\text{Specular, Diffuse}\}}, \tag{13}$$

where $\hbar_r$ represents the total channel gain, while B, P_T, and $\mathcal{N}$ represent the system bandwidth, the optical transmit power, and the noise power spectral density, respectively. Note that, although broadcasting the same signal by all Txs is effective in handling cases of large overlapping between coverage areas of the Txs, it comes at the cost of degradations in the spectral efficiency. For evaluating the fairness performance of the system, we adopt Jain's FI with respect to the user achievable throughput, which can be expressed as [35]:

$$\text{FI} = \frac{1}{N_r}\frac{\left(\sum_{i=1}^{N_r} R_i\right)^2}{\sum_{i=1}^{N_r} R_i^2}. \tag{14}$$

To achieve the optimization goals, we consider utility function in which the weighted sum of the network sum rate and FI are related as follows:

$$\frac{(1-\eta)}{\mu_1}\sum_{i=1}^{N_r} R_i + \frac{\eta}{\mu_2} \times \text{FI}, \tag{15}$$

where η is the multi-objective weight ranging between 0 and 1, indicating the preference assigned for each objective utility. Particularly, $\eta = 0$ would result in optimizing the system for maximizing sum rate, while $\eta = 1$ would lead to optimizing the system to maximize FI. The values of μ_1 and μ_2 are used to normalize the two objective functions to balance and control their contributions [36], where μ_1 is obtained by setting $\eta = 0$ and calculating the average sum rate over 1000 independent realizations, while μ_2 is obtained by setting $\eta = 1$ and calculating the average FI over 1000 independent realizations. In general, assigning values for η between 0 and 1 will result in varying the balance between the two objective functions. In the following subsections, we discuss optimizing the utility function defined for the specular and diffuse reflecting RISs.

A. SPECULAR REFLECTING RIS

As mentioned in Section II, since each specular reflecting RIS element is considered to serve one Tx and one Rx at a time, the optimization problem can be reduced to finding the optimal associations for the RIS elements, which is expressed by the association matrices $\mathbf{Q}$ and $\mathbf{Z}$. Once the associations are decided, a reverse lookup table can be utilized to adjust the RIS elements orientations [12]. Here, the reflected components through the RIS array towards the r^{th} Rx can be expressed as:

$$\sum_{l=1}^{N_t} (\mathbf{q}_l \odot \mathbf{z}_r)^T \mathbf{h}_{l,r}^{\text{RIS}}, \tag{16}$$

and the problem in (15) can be then formulated as:

$$\max_{\mathbf{Q},\mathbf{Z}} \quad \frac{(1-\eta)}{\mu_1} \sum_{i=1}^{N_r} R_i(\mathbf{Q},\mathbf{Z}) + \quad \frac{\eta}{\mu_2} \times \text{FI}(\mathbf{Q},\mathbf{Z}), \tag{17a}$$

s.t.:

$$q_{n,l} \in \{0,1\}; \quad \forall n, \quad \forall l, \tag{17b}$$

$$z_{n,r} \in \{0,1\}; \quad \forall n, \quad \forall r, \tag{17c}$$

$$\sum_{l=1}^{N_t} q_{n,l} \quad \leq \quad 1; \quad \forall n, \tag{17d}$$

$$\sum_{r=1}^{N_r} z_{n,r} \quad \leq \quad 1; \quad \forall n, \tag{17e}$$

where (17d) and (17e) ensure the association of one Tx and one Rx at a time with each RIS element. Here, the number of possible combinations in the solution space of the resulting non-linear non-convex integer programming problem, which is NP-hard, is $2^{N_t N_{\text{RIS}}} \times 2^{N_r N_{\text{RIS}}}$. To simplify the search space, we introduce two auxiliary association vectors $\mathbf{u} = [u_1, \ldots, u_{N_{\text{RIS}}}]$ and $\mathbf{w} = [w_1, \ldots, w_{N_{\text{RIS}}},]$ with elements representing the indices of the Txs and Rxs served by each RIS element, respectively. More specifically, $u_n = l$ and $w_n = r$ indicate that the n^{th} RIS element is associated to the l^{th} Tx and the r^{th} Rx, respectively, thus accounting for the corresponding associations in $\mathbf{Q}$ and $\mathbf{Z}$ while satisfying the constraints (17d) and (17e). The problem can be then expressed as:

$$\max_{\mathbf{u},\mathbf{w}} \quad \frac{(1-\eta)}{\mu_1} \sum_{i=1}^{N_r} R_i(\mathbf{u},\mathbf{w}) + \frac{\eta}{\mu_2} \times \text{FI}(\mathbf{u},\mathbf{w}), \tag{18a}$$

s.t.:

$$u_n \in \{1, \ldots, N_t\} \quad \forall n, \tag{18b}$$

$$w_n \in \{1, \ldots, N_r\} \quad \forall n, \tag{18c}$$

where the number of possible combinations in the solution space is $N_t^{N_{\text{RIS}}} \times N_r^{N_{\text{RIS}}}$. Given the non-convexity of the handled integer programming problem of finding the set of combinations that maximizes the objective function in (18), we consider solving it using GA-based optimization approach, which is known to efficiently handle integer-based problems [37].

Algorithm 1 GA-Based Specular Reflecting RISs Optimization

Input: S_p, N_{Gen}, H
Output: Optimal associations for RIS elements

```
Generate a random initial population of size S_p
Calculate the association vectors u and w
Set i_g = 1
while i_g ≤ N_Gen do
    Select random association vectors from old generation
    Apply crossover with probability P_c
    Carry out mutation operation with probability P_m
    Evaluate the solution using (18)
    Select the elite association vector
    Set i_g = i_g + 1
end while
```

GA is an evolutionary stochastic-based optimization technique inspired by the fitness improvement through evolution in the biological systems [38], which has shown efficiency in solving optical wireless communications problems [18], [25]. In GA, the solutions are represented by strings (chromosomes), which consist of sets of elements (genes) that point to possible values for the considered variables in the optimization problem [38].

The proposed optimization of specular reflecting RIS arrays using GA starts with considering an initial chromosomes population, which denotes a random subset of the possible solutions. In each of the algorithm iterations, two operations could be adopted to control the next generation, namely cross-over and mutation. In crossover, the offspring chromosomes are generated by exchanging information between parent chromosomes. For the mutation operation, the algorithm changes the offspring chromosomes, which can be carried out by randomly selecting and varying the information of chromosomes. At each iteration, the fitness values are evaluated where the solutions with best fitness values are considered in the next iteration (i.e., the chromosomes (associations) whose fitness values are better are kept). The pseudocode of the algorithm is presented in Algorithm 1 for a population size (S_p), number of generations (N_{Gen}), network channel matrix (H), and probabilities of crossover and mutation of $\mathcal{P}_c$ and $\mathcal{P}_m$, respectively.

1) COMPLEXITY AND CONVERGENCE ANALYSIS

The computational complexity of Algorithm 1 is described as follows: assuming the number of variables of the problem is Q, generating the random initial population of size S will require $\mathcal{O}(QS)$ operations. For the worst case complexity to complete the algorithm, it requires $\mathcal{O}(N_{Gen}(QS + QS + Q))$ operations. Therefore, the overall complexity is on the order of $\mathcal{O}(N_{Gen}QS)$. Figure 5, shows the convergence rate of Algorithm 1. The result demonstrates that the algorithm

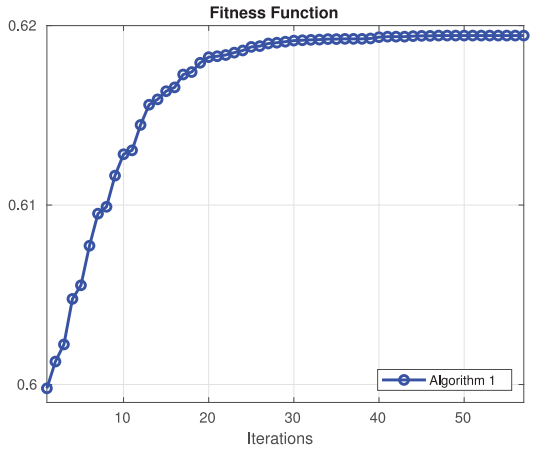

FIGURE 5. The convergence rate of Algorithm 1. The Algorithm converges to the optimized solution within around 40 iterations.

converges to the optimized solution within around 40 iterations.

B. DIFFUSE REFLECTING RIS

As discussed in Section II, the variables used for the optimization of the diffuse reflecting RIS array are the angles that control the orientations of the RIS elements (i.e., vectors of angles of roll $\boldsymbol{\alpha} = [\alpha_1, \ldots, \alpha_{N_{\text{RIS}}}]$ and yaw $\boldsymbol{\beta} = [\beta_1, \ldots, \beta_{N_{\text{RIS}}}]$). Here, the problem could be formulated as follows:

$$\max_{\boldsymbol{\alpha},\boldsymbol{\beta}} \quad \frac{(1-\eta)}{\mu_1} \sum_{i=1}^{N_r} R_i(\alpha_i, \beta_i) + \frac{\eta}{\mu_2} \times \text{FI}(\boldsymbol{\alpha}, \boldsymbol{\beta}), \quad (19a)$$

s.t.:

$$-\frac{\pi}{2} \leq \alpha_j \leq \frac{\pi}{2}, \quad j \in \{1, \ldots, N_{\text{RIS}}\}, \quad (19b)$$

$$-\frac{\pi}{2} \leq \beta_j \leq \frac{\pi}{2}, \quad j \in \{1, \ldots, N_{\text{RIS}}\}, \quad (19c)$$

where the constraints (19b) and (19c) ensure the feasibility of the orientations of the RIS elements. For RIS array with N_{RIS} elements, the optimization problem in (19) have $2N_{\text{RIS}}$ variables and $2N_{\text{RIS}}$ constraints. Again, given the non-convexity of the problem, we solve it using PSO-based optimization approach, which is known to efficiently handle problems with continuous solution space [39].

PSO is a stochastic optimization technique inspired by the movement of swarms in nature (i.e., swarms of birds and bees) [40] and has been widely used to solve problems related to VLC [22], [26], [27]. In PSO, a swarm of particles is considered to look for the optimal solution in the search space formed by the possible combinations of the variables, where each particle is influenced by the best solution it discovered (Pbest) and the best solution discovered by all members of the swarm (Gbest) until converging to the best point (optimized solution).

The considered optimization of RIS elements orientations using PSO algorithm begins with assuming a swarm of N_P particles randomly located in the search space, which is explored over N_{it} iterations. The positions found by the particles in the search space (solutions) are evaluated using the utility function, where the next moves of the particles are decided based on their current move as well as the Pbest and Gbest solutions. In particular, for a particle p at iteration $\tau+1$ in a K dimensional search space, the algorithm updates the particle position vector $\boldsymbol{x_p} = [x_{p1}, \ldots, x_{pK}]$ and velocity vector $\boldsymbol{v_p} = [v_{p1}, \ldots, v_{pK}]$, while being influenced by the Pbest vector $\boldsymbol{Pbest_p} = [Pbest_{p1}, \ldots, Pbest_{pK}]$ and Gbest vector $\boldsymbol{Gbest} = [Gbest_1, \ldots, Gbest_K]$, where for variable k:

$$v_{pk}^{\tau+1} = \varpi^{\tau} \times v_{pk}^{\tau} + c_1 \times rp \times \left(Pbest_{pk} - x_{pk}^{\tau}\right) + c_2 \times rg \times \left(Gbest_k - x_{pk}^{\tau}\right), \quad (20a)$$

$$x_{pk}^{\tau+1} = x_{pk}^{\tau} + v_{pk}^{\tau+1} \Delta t. \quad (20b)$$

Here, ϖ^{τ} represents the inertial factor that controls the contribution of the particle old velocity to the new velocity calculations, rp and rg are random numbers valued between 0 and 1, and c_1 and c_2 are weights that control the contributions of Pbest and Gbest solutions to the utility function, respectively. Note that, Δt is a time step that is set to 1. The algorithm pseudocode is explained in Algorithm 2. The worst case complexity of the algorithm is $\mathcal{O}(N_{it} K N_p)$.

Algorithm 2 PSO-Based Diffuse Reflecting RISs Optimization

Input: N_p, N_{it}, H
Output: Optimal orientations for RIS elements

```
Generate random initial population of size N_P
Calculate the associated orientation vectors α and β
Set τ = 1
while no convergence And τ ≤ N_it do
    for p = 1:N_P do
        Evaluate x_pk^τ using the utility function
        Update Pbest_pk and Gbest_k
        Calculate v_pk^{τ+1} and x_pk^{τ+1}
        Set τ = τ + 1
    end for
end while
```

1) COMPLEXITY AND CONVERGENCE ANALYSIS

The computational complexity of Algorithm 2 is described as follows: assuming that the number of decision variables is S, generating the initial set of solutions for all particles requires $\mathcal{O}(SN_P)$ operations. Computing the fitness function and updating the velocity of the particles requires $\mathcal{O}(N_P)$ operations. The worst-case complexity for evaluating the fitness function for all particles and updating the destination is $\mathcal{O}(N_P N_{it})$ and $\mathcal{O}(N_P N_{it})$, respectively. The worst case complexity for updating the solution sets according to (20) is $\mathcal{O}(SN_P N_{it})$. Hence, the overall complexity of finding a solution using Algorithm 2 is $\approx \mathcal{O}(SN_P N_{it})$. Figure 6 shows the convergence rate of Algorithm 2. The result demonstrates

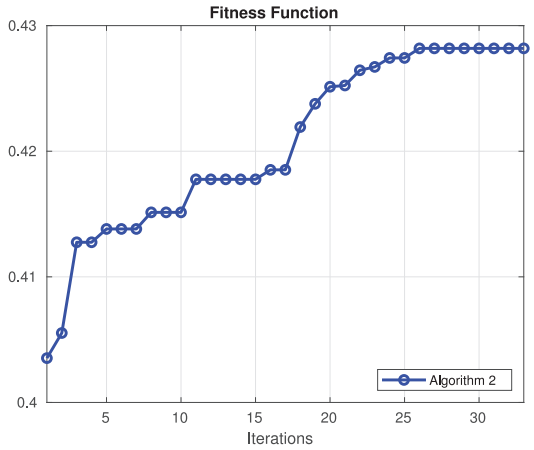

FIGURE 6. The convergence rate of Algorithm 2. The Algorithm converges to the optimized solution within 27 iterations.

TABLE 2. Simulation parameters.

Parameter	Value
Transmit optical power (P_T)	1.584 W
Lambertian order (m)	1
System bandwidth (BW)	10 MHz
Specular reflecting RIS element reflection coefficient (δ)	0.90
Diffuse reflecting RIS element reflection coefficient (ρ)	0.90
Number of users (N_r)	4
Rx FOV	60°
Rx area (A_r)	1 cm^2
Concentrator refractive index (n_{ri})	1.5
PD responsivity (ξ_r)	0.4 A/W
Mean of Rx polar angle θ (ϱ_{θ_o})	41.39°
Variance of Rx polar angle (b_{θ_o})	7.68°
Noise Power spectral density ($\mathcal{N}$)	10^{-21}

that the algorithm converges to the optimized solution within 27 iterations.

IV. PERFORMANCE EVALUATION

To evaluate the performance of the proposed optimization of specular and diffuse reflecting RISs, we consider an indoor multi-user VLC system, where the room dimensions are 5m × 5m × 3m and the point $(0, 0, 0)$ is assumed to be at the center of the ground plane. Two LED-based luminaires that act as Txs are placed at $(0, -1, 3)$ and $(0, 1, 3)$ m, while the user devices are randomly located at height of 0.85 m above the ground plane. Note that, random orientations of the user devices are considered following the model discussed in Section II-C. A square RIS array is assumed to be placed on one of the room walls and is centered at $(2.5, 0, 1.5)$ m, where each RIS element has a dimension of 10 cm × 10 cm. Note that, the NLOS calculations only account for the reflections from the RIS arrays, where the results are averaged over 1000 random realizations for user locations and orientations. The main simulation parameters are provided in Table 2.

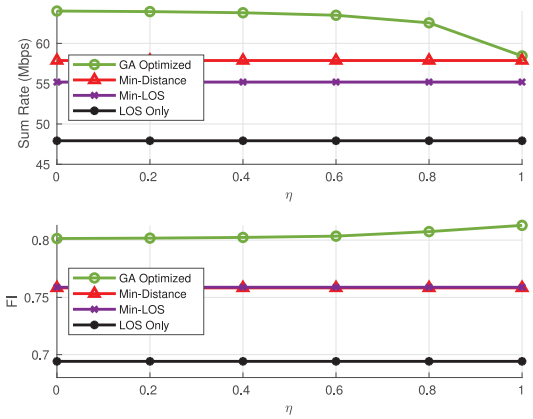

FIGURE 7. Effect of varying the multi-objective function weight on the optimization of specular reflecting RIS elements in terms of sum rate and FI.

A. SPECULAR REFLECTING RIS

As highlighted in (18), the multi-objective weight η impacts the contributions of sum rate and FI terms in the utility function. This implies careful design of η to maximize the efficiency of resource utilization in terms of RIS elements associations, which is reflected in the users achievable throughputs and homogeneity between individual user performances. Therefore, we start with studying the effect of varying η on the network performance while considering 100 specular reflecting RIS elements and compare the results with those of two non-optimized association techniques. In the first, the RIS assignments are based on associating the Tx and Rx closest in distance to the RIS element, which we refer to as "min-distance". For the second scheme, the assignment is based on associating the Tx closest in distance to the RIS element with the user with the lowest LOS channel gain, which we refer to as "min-LOS". Figure 7 illustrates the effect of increasing η on both of sum rate and FI performances. As highlighted, increasing η would result in higher contribution of the FI term and lower contribution of the sum rate term. As we target striking a balance between the two terms, we choose $\eta = 0.8$ for the following simulations.

To present the impact of varying the number of specular reflecting RIS elements on VLC network performance, Fig. 8 shows the results of comparing the proposed optimization with case of relying only on LOS (i.e., no RISs), as well as cases of min-distance and min-LOS algorithms, in terms of sum rate and FI. Generally, exploiting the spatial diversity provided by the RIS elements enhanced the NLOS channel gains, which resulted in improved sum rate compared to the case of considering only LOS components. In addition, the proposed optimization of specular reflecting RIS elements resulted in performance enhancements in terms of sum rate, where the results indicate that utilizing 144 RIS elements improved the performance by 40%, 11%, and 17% compared with cases of considering only LOS, min-distance, and min-LOS schemes, respectively. Moreover, the proposed optimization resulted in improvements in terms of FI of 20%,

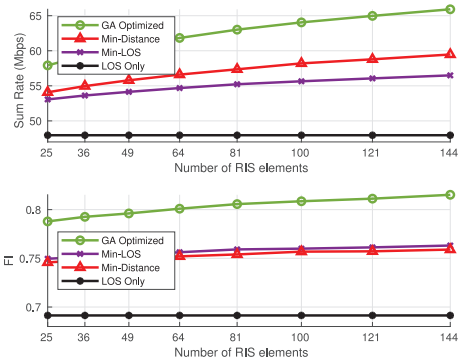

FIGURE 8. Comparison between the GA-based optimization of specular reflecting RIS elements with cases of considering LOS only, min-distance, and min-LOS algorithms in terms of sum rate and FI performances.

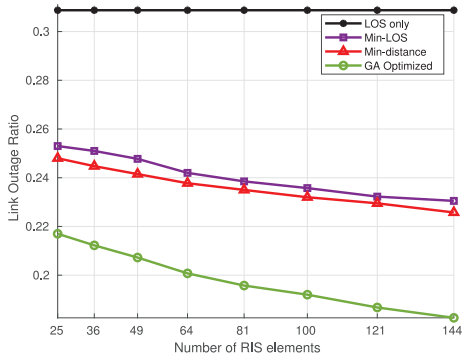

FIGURE 9. Comparison between the GA-based optimization of specular reflecting RIS elements with cases of considering LOS only, min-distance, and min-LOS algorithms in terms of link outage ratio.

9% and 8% compared to cases of LOS only, min-distance, and min-LOS, respectively.

To highlight the impact of using specular reflecting RIS arrays on VLC link reliability, we assess the performance in terms of link outage ratio, which we calculate based on comparing the number of users with achievable throughput below a certain threshold, $R_{th} = 10$ Mbps, to the total number of users. Here, since we target improving the minimum individual user performances rather than the network sum rate, we focus on maximizing the FI (i.e., we set $\eta = 1$). Figure 9 compares the link outage ratio for the optimized case with the cases of considering LOS only, min-distance, and min-LOS algorithms. It can be observed that, as expected, the link outage ratio improved with the presence of RISs due to the spatial diversity in the system. In addition, the link outage ratio decreased by considering higher number of RIS elements as each element provides an additional NLOS path for the links between the associated Txs and Rxs. It is also noted that optimizing the RIS elements resulted in improved performance compared to the min-distance and min-LOS algorithms, as maximizing the fairness between individual user performances could results in higher association for the RIS elements with the users with low achievable throughput to decrease the performance gaps between the individual user performances, hence, reducing the probability that user achievable throughput falls below the outage threshold. Particularly, for the case of 144 RIS elements, optimizing the RIS elements resulted in 42%, 22%, and 20% reduction in the link outage ratio compared to the cases of LOS only, min-LOS, and min-distance, respectively.

B. DIFFUSE REFLECTING RIS

To highlight the impact of varying η on the optimization of the diffuse reflecting RIS elements in (19), we start by comparing the performance with cases of fixed (i.e., yaw and roll angles equal to 0°) and random orientations while assuming 100 RIS elements. Given the ability of the diffuse reflecting RIS elements to support connectivity at low alignment requirements, we highlight their impact

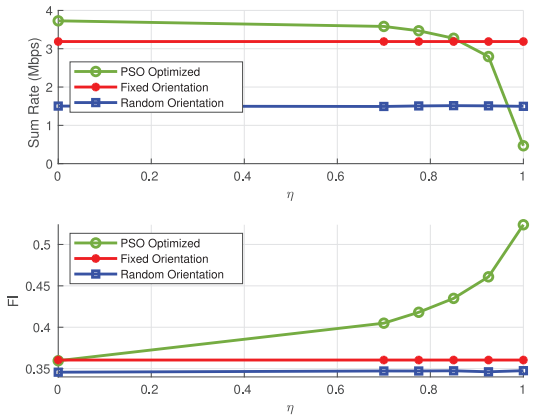

FIGURE 10. Effect of varying the multi-objective function weight on the optimization of diffuse reflecting RIS elements in terms of sum rate and FI.

on improving the VLC link reliability by evaluating the performance in cases of LOS blockage. Figure 10 shows the effect of increasing η on the sum rate and FI performances, which decreased and increased, respectively, due to the variations of the contributions of the first and second terms in (19). To balance the contributions of the terms in the objective function, we choose $\eta = 0.6$ in the following simulations.

To assess the effect of varying the number of diffuse RIS elements per array on VLC network performance, we compare in Fig. 11 the performance of the proposed optimization with cases of fixed and random RIS orientations in terms of sum rate and FI. As expected, increasing the number of RIS elements improved the sum rate performance due to increase in number of NLOS paths between the Txs and Rxs. In addition, the results show that the proposed optimization of the diffuse reflecting RIS elements outperformed cases of fixed and random orientations. Specifically, for the case of 144 RIS elements, the proposed optimization offered sum rate improvements of 100% and 5% compared to random and fixed RIS orientation schemes, respectively. Also, it improved the FI performance by 15% compared to case of random RIS orientations and 10% in comparison with case of fixed RIS orientations.

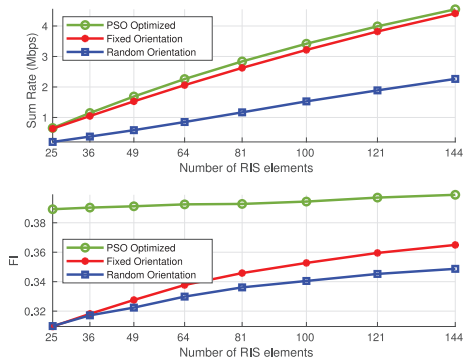

FIGURE 11. Comparison between the PSO-based optimization of diffuse reflecting RIS elements with cases of fixed and random RIS elements orientations in terms of sum rate and FI.

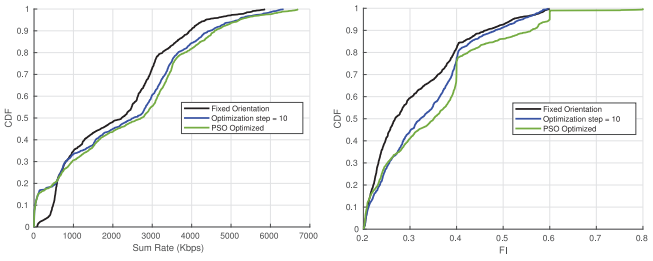

FIGURE 12. CDF of average (a) sum rate and (b) FI performances for cases of optimizing the diffuse reflecting RIS elements and adopting fixed RIS elements orientations.

One of the advantages of relying on diffuse reflecting RISs in VLC system is minimizing the alignment requirements between the Txs and Rxs, which opens the door for their use to improve the network performance in cases of user mobility [4]. In particular, as the reflected beams by the RIS elements are diffused in multiple directions, contrary to the specular reflecting RIS elements, the mobile users in VLC networks could be able to receive the reflections via the RIS elements while requiring limited alignment requirements. To evaluate the system performance in cases of handling mobile users, we consider RIS-assisted indoor VLC system where user locations are generated using random waypoint (RWP) mobility model [41], with separation between successive user positions of 0.1 s and maximum user velocity of 0.5 m/s. The performance of the proposed optimization is compared with cases of decreasing the optimization rate (carrying out optimization every 10 time steps (T_{step})) and adopting fixed RIS orientations. Figures 12(a) and 12(b) show the cumulative distribution function (CDF) of average sum rate and FI performances over 1000 time steps for case of considering 100 RIS elements. The results show that optimizing the diffuse reflecting RIS elements resulted in highest sum rate and FI performances, followed by case of decreasing the optimization rate, which highlights the ability of the proposed optimization to improve the performance at lower complexity. To further highlight the impact of varying the rate of optimization on system performance, Figs. 13(a) and 13(b) illustrate the differences in average sum rate and FI with the decrease in optimization rate over 30 values of T_{step}. The results highlight the robustness of the proposed optimization (e.g., achieving sum rate difference around 100 Kbps and FI difference less than 0.04 in case of carrying out the optimization every 5 and 10 time steps, respectively), benefitting from the diffuse reflections by the RIS elements. It also highlights the trade-off between decreasing the computational complexity represented by the optimization rate and the degradation in network performance, which could be considered for adapting to the system needs.

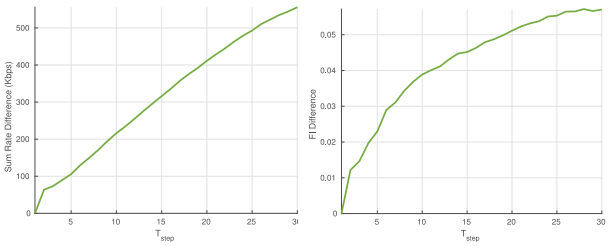

FIGURE 13. Impact of varying the optimization rate on (a) sum rate and (b) FI performances.

C. SPECULAR VS DIFFUSE REFLECTING RIS

The results in Sections IV-A and IV-B highlight the ability of both of specular and diffuse reflecting RISs to improve system performance, where by comparing the results, the following key differences are highlighted:

- specular reflecting RISs provide superior performance in terms of sum-rate compared to the diffuse reflecting RISs. This is attributed to the concentration of the reflected beams by specular reflection towards the Rx, as the reflected beams by diffuse reflection are scattered in the communications environment resulting in lower received power levels. The dependence of the NLOS channel gain reflected by the diffuse reflecting RIS elements in equation (7) on $\cos(\theta_{l,n})$, $\cos(\Phi_{n,r})$, and the square of $d_{l,n}$ and $d_{n,r}$ in the denominator results in lower channel gain compared to the square of summation of $d_{l,n}$ and $d_{n,r}$ in the denominator of equation (5) for the specular reflecting RIS elements.
- diffuse reflecting RISs have less alignment requirements, as a result of the scattering of the reflected beams in the communications environment, which makes them more suitable for applications involving user mobility and/or inaccuracy in locating Rxs. Also, this makes them suitable for use cases where there is a need for decreasing the optimization complexity and/or pilot overhead associated with channel estimation. The results in Section IV-B highlights the trade-off between decreasing the optimization rate (complexity) and system performance.

V. CONCLUSION

In this work we proposed optimization of the specular and diffuse reflecting RISs in indoor VLC systems to target improving the network sum rate and fairness. GA-based optimization was considered for optimizing the specular reflecting RISs, where the results have shown improvements in terms of sum rate, FI, and link outage ratio compared to non-optimized cases. The results also highlighted the flexibility of the proposed optimization to adapt to the network needs by varying the objective function weights. PSO-based optimization was then considered for optimizing the diffuse reflecting RIS elements, which was further extended to cases of handling mobile users, where the results presented improvements in system performance in terms of sum rate and FI. We also highlighted the ability of the diffuse reflecting RIS arrays to improve VLC network reliability in cases of LOS blockage at low alignment complexity, and the trade-off between decreasing the optimization rate and improving the network performance. As the number of RIS elements controls the number of variables and subsequently the complexity of the RIS array optimization, as highlighted in the complexity analysis of Algorithms 1 and 2, a balance is needed to address the trade-off between the RIS array size (network performance) and the optimization complexity.

Future research directions include investigating (i) the optimization of the RISs distributions in the communications environment; (ii) the use of RIS arrays that simultaneously supports specular and diffuse reflections to enable more degrees of freedom in the optimization of the network performance, which could be realized by using both types of RIS elements within the same array; and (iii) the consideration of the impacts of dimming and using different multiple access techniques in multi-cellular VLC systems on cell-center and cell-edge users.

REFERENCES

[1] Z. Ghassemlooy, L. N. Alves, S. Zvanovec, and M. A. Khalighi, *Visible Light Communications: Theory and Applications*. Boca Raton, FL, USA: CRC-Press, 2017.

[2] S. Aboagye, A. R. Ndjiongue, T. M. N. Ngatched, O. A. Dobre, and H. V. Poor, "RIS-assisted visible light communication systems: A tutorial," *IEEE Commun. Surveys Tuts.*, vol. 25, no. 1, pp. 251–288, 1st Quart., 2023.

[3] H. Abumarshoud, L. Mohjazi, O. A. Dobre, M. Di Renzo, M. A. Imran, and H. Haas, "LiFi through reconfigurable intelligent surfaces: A new frontier for 6G?" *IEEE Veh. Technol. Mag.*, vol. 17, no. 1, pp. 37–46, Mar. 2022.

[4] S. Abdeljabar, M. W. Eltokhey, and M.-S. Alouini, "Reconfigurable intelligent surfaces for outdoor visible light communications," Submitted for Publication.

[5] O. Maraqa, S. Aboagye, and T. M. N. Ngatched, "Optical STAR-RIS-aided VLC systems: RSMA versus NOMA," *IEEE Open J. Commun. Soc.*, vol. 5, pp. 430–441, 2024.

[6] O. Maraqa and T. M. N. Ngatched, "Optimized design of joint mirror array and liquid crystal-based RIS-aided VLC systems," *IEEE Photon. J.*, vol. 15, no. 4, pp. 1–11, Aug. 2023.

[7] A. M. Abdelhady, A. K. S. Salem, O. Amin, B. Shihada, and M.-S. Alouini, "Visible light communications via intelligent reflecting surfaces: Metasurfaces vs mirror arrays," *IEEE Open J. Commun. Soc.*, vol. 2, pp. 1–20, 2020.

[8] A. Yesilkaya, H. Abumarshoud, and H. Haas, "Optical wireless communications using intelligent walls," in *Intelligent Reconfigurable Surfaces (IRS) for Prospective 6G Wireless Networks*. Hoboken, NJ, USA: Wiley, Inc., 2023, pp. 233–274.

[9] S. Aboagye, T. M. Ngatched, O. A. Dobre, and A. R. Ndjiongue, "Intelligent reflecting surface-aided indoor visible light communication systems," *IEEE Commun. Lett.*, vol. 25, no. 12, pp. 3913–3917, Dec. 2021.

[10] Z. Liu, F. Yang, S. Sun, J. Song, and Z. Han, "Sum rate maximization for NOMA-based VLC with optical intelligent reflecting surface," *IEEE Wireless Commun. Lett.*, vol. 12, no. 5, pp. 848–852, May 2023.

[11] S. Sun, F. Yang, and J. Song, "Sum rate maximization for intelligent reflecting surface-aided visible light communications," *IEEE Commun. Lett.*, vol. 25, no. 11, pp. 3619–3623, Nov. 2021.

[12] S. Sun, F. Yang, J. Song, and Z. Han, "Joint resource management for intelligent reflecting surface–aided visible light communications," *IEEE Trans. Wireless Commun.*, vol. 21, no. 8, pp. 6508–6522, Aug. 2022.

[13] Q. Wu, J. Zhang, and J.-N. Guo, "Position design for reconfigurable intelligent-surface-aided indoor visible light communication systems," *Electronics*, vol. 11, no. 19, p. 3076, 2022.

[14] Q. Wu, J. Zhang, Y. Zhang, G. Xin, and J. Guo, "Configuring reconfigurable intelligent surface for parallel MIMO visible light communications with asymptotic capacity maximization," *Appl. Sci.*, vol. 13, no. 1, p. 563, 2022.

[15] C. Liu, L. Yu, X. Yu, J. Qian, Y. Wang, and Z. Wang, "Capacity analysis of RIS-assisted visible light communication systems with hybrid NOMA," in *Proc. IEEE Global Commun. Conf. (GLOBECOM) Workshops*, 2022, pp. 118–123.

[16] Q. Wu, J. Zhang, and J. Guo, "Capacity maximization for reconfigurable intelligent surface-aided MISO visible light communications," *Photonics*, vol. 9, no. 7, p. 487, 2022.

[17] A. Al Hammadi, L. Bariah, S. Muhaidat, M. Al-Qutayri, P. C. Sofotasios, and M. Debbah, "Deep Q-learning based resource management in IRS-assisted VLC systems," *IEEE Trans. Mach. Learn. Commun. Netw.*, vol. 2, pp. 34–48, 2024. [Online]. Available: https://ieeexplore.ieee.org/document/10299678

[18] H. Abumarshoud, B. Selim, M. Tatipamula, and H. Haas, "Intelligent reflecting surfaces for enhanced NOMA-based visible light communications," in *Proc. IEEE Int. Conf. Commun. (ICC)*, 2022, pp. 571–576.

[19] X.-D. Shi, L.-H. Hong, P.-F. Yu, J.-W. Shi, N. Liu, and J.-Y. Wang, "Performance analysis and parameter optimization for intelligent reflecting mirror array-aided visible light communications," *J. Opt. Soc. Am. A*, vol. 39, no. 10, pp. 1839–1848, 2022.

[20] S. Sun, F. Yang, J. Song, and R. Zhang, "Intelligent reflecting surface for MIMO VLC: Joint design of surface configuration and transceiver signal processing," *IEEE Trans. Wireless Commun.*, vol. 22, no. 9, pp. 5785–5799, Sep. 2023.

[21] H. Abumarshoud, C. Chen, I. Tavakkolnia, H. Haas, and M. A. Imran, "Intelligent reflecting surfaces for enhanced physical layer security in NOMA VLC systems," in *Proc. IEEE Int. Conf. Commun. (ICC)*, 2023, pp. 3284–3289.

[22] L. Qian, X. Chi, L. Zhao, and A. Chaaban, "Secure visible light communications via intelligent reflecting surfaces," in *Proc. IEEE Int. Conf. Commun. (ICC)*, 2021, pp. 1–6.

[23] D. A. Saifaldeen, B. S. Ciftler, M. M. Abdallah, and K. A. Qaraqe, "DRL-based IRS-assisted secure visible light communications," *IEEE Photon. J.*, vol. 14, no. 6, pp. 1–9, Dec. 2022.

[24] S. Sun, F. Yang, J. Song, and Z. Han, "Optimization on multiuser physical layer security of intelligent reflecting surface-aided VLC," *IEEE Wireless Commun. Lett.*, vol. 11, no. 7, pp. 1344–1348, Jul. 2022.

[25] M. D. Higgins, R. J. Green, and M. S. Leeson, "A genetic algorithm method for optical wireless channel control," *J. Lightw. Technol.*, vol. 27, no. 6, pp. 760–772, Mar. 15, 2009.

[26] M. S. Demir, S. M. Sait, and M. Uysal, "Unified resource allocation and mobility management technique using particle swarm optimization for VLC networks," *IEEE Photon. J.*, vol. 10, no. 6, pp. 1–9, Dec. 2018.

[27] M. W. Eltokhey, M.-A. Khalighi, and Z. Ghassemlooy, "UAV location optimization in MISO ZF pre-coded VLC networks," *IEEE Wireless Commun. Lett.*, vol. 11, no. 1, pp. 28–32, Jan. 2022.

[28] M. W. Eltokhey, M. A. Khalighi, A. S. Ghazy, and S. Hranilovic, "Hybrid NOMA and ZF pre-coding transmission for multi-cell VLC networks," *IEEE Open J. Commun. Soc.*, vol. 1, pp. 513–526, 2020.

[29] K. Lee, H. Park, and J. R. Barry, "Indoor channel characteristics for visible light communications," *IEEE Commun. Lett.*, vol. 15, no. 2, pp. 217–219, Feb. 2011.
[30] T. Komine and M. Nakagawa, "Fundamental analysis for visible-light communication system using LED lights," *IEEE Trans. Consum. Electron.*, vol. 50, no. 1, pp. 100–107, Feb. 2004.
[31] V. Jamali, H. Ajam, M. Najafi, B. Schmauss, R. Schober, and H. V. Poor, "Intelligent reflecting surface assisted free-space optical communications," *IEEE Commun. Mag.*, vol. 59, no. 10, pp. 57–63, Oct. 2021.
[32] A. M. Abdelhady, O. Amin, A. K. S. Salem, M.-S. Alouini, and B. Shihada, "Channel characterization of IRS-based visible light communication systems," *IEEE Trans. Commun.*, vol. 70, no. 3, pp. 1913–1926, Mar. 2022.
[33] M. D. Soltani, A. A. Purwita, Z. Zeng, H. Haas, and M. Safari, "Modeling the random orientation of mobile devices: Measurement, analysis and LiFi use case," *IEEE Trans. Commun.*, vol. 67, no. 3, pp. 2157–2172, Mar. 2019.
[34] J.-B. Wang, Q.-S. Hu, J. Wang, M. Chen, and J.-Y. Wang, "Tight bounds on channel capacity for dimmable visible light communications," *J. Lightw. Technol.*, vol. 31, no. 23, pp. 3771–3779, Dec. 1, 2013.
[35] R. K. Jain, D.-M. W. Chiu, and W. R. Hawe, "A quantitative measure of fairness and discrimination," Eastern Res. Lab., Hudson, MA, USA, Rep. TR-301, 1984.
[36] J. Woo, C. Song, and I. Lee, "Sum rate and fairness optimization for intelligent reflecting surface aided multiuser systems," *IEEE Trans. Veh. Technol.*, vol. 70, no. 12, pp. 13436–13440, Dec. 2021.
[37] M. Sakawa, *Genetic Algorithms and Fuzzy Multiobjective Optimization*, vol. 14. New York, NY, USA: Springer, 2002.
[38] E. Elbeltagi, T. Hegazy, and D. Grierson, "Comparison among five evolutionary-based optimization algorithms," *Adv. Eng. Inform.*, vol. 19, no. 1, pp. 43–53, 2005.
[39] D. Sha and C.-Y. Hsu, "A hybrid particle swarm optimization for job shop scheduling problem," *Comput. Ind. Eng.*, vol. 51, no. 4, pp. 791–808, 2006.
[40] A. Ratnaweera, S. K. Halgamuge, and H. C. Watson, "Self-organizing hierarchical particle swarm optimizer with time-varying acceleration coefficients," *IEEE Trans. Evol. Comput.*, vol. 8, no. 3, pp. 240–255, Jun. 2004.
[41] C. Bettstetter, H. Hartenstein, and X. Pérez-Costa, "Stochastic properties of the random waypoint mobility model," *Wireless Netw.*, vol. 10, pp. 555–567, Sep. 2004.

SALAH ABDELJABAR (Student Member, IEEE) received the B.Sc. degree in electrical engineering from The University of Jordan, Amman, Jordan, in 2019, and the M.Sc. degree in electrical and computer engineering from the King Abdullah University of Science and Technology, Thuwal, Saudi Arabia, in 2023, where he is currently pursuing the Ph.D. degree. His research interests include optical wireless communications systems and reconfigurable intelligent surfaces.

MAHMOUD WAFIK ELTOKHEY (Member, IEEE) received the B.Sc. and M.Sc. degrees from the Department of Electronics and Communications Engineering, Mansoura University, Mansoura, Egypt, in 2012 and 2016, respectively, and the Ph.D. degree from the Institut Fresnel, École Centrale Marseille, Marseille, France, in 2021. He was an Early Stage Researcher with the H2020 ITN MSCA VisIoN Project from 2018 to 2021. He is currently a Postdoctoral Fellow with the Communication Theory Lab, King Abdullah University of Science and Technology, Thuwal, Saudi Arabia. His current research interests include optical wireless communications and adaptive systems.

MOHAMED-SLIM ALOUINI (Fellow, IEEE) was born in Tunis, Tunisia. He received the Ph.D. degree in electrical engineering from the California Institute of Technology, Pasadena, CA, USA, in 1998. He served as a Faculty Member with the University of Minnesota, Minneapolis, MN, USA, then with Texas A&M University at Qatar, Doha, Qatar, before joining the King Abdullah University of Science and Technology, Thuwal, Makkah, Saudi Arabia, as a Professor of Electrical Engineering in 2009. His current research interests include the modeling, design, and performance analysis of wireless communication systems.